AIP | Review of Scientific Instruments

Single-shot velocity-map imaging of attosecond light-field control at kilohertz rate

F. Süßmann, S. Zherebtsov, J. Plenge, Nora G. Johnson, M. Kübel, A. M. Sayler, V. Mondes, C. Graf, E. Rühl, G. G. Paulus, D. Schmischke, P. Swrschek, and M. F. Kling

Citation: Review of Scientific Instruments **82**, 093109 (2011); doi: 10.1063/1.3639333
View online: http://dx.doi.org/10.1063/1.3639333
View Table of Contents: http://scitation.aip.org/content/aip/journal/rsi/82/9?ver=pdfcov
Published by the AIP Publishing

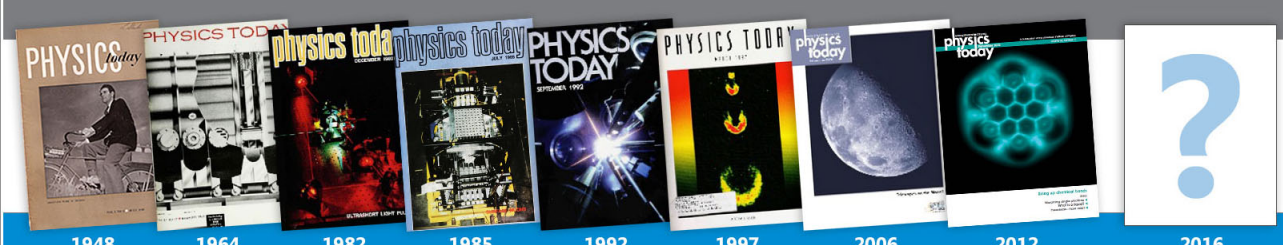

Single-shot velocity-map imaging of attosecond light-field control at kilohertz rate

F. Süßmann,[1] S. Zherebtsov,[1] J. Plenge,[2] Nora G. Johnson,[1,3] M. Kübel,[1] A. M. Sayler,[4,5] V. Mondes,[2] C. Graf,[2] E. Rühl,[2] G. G. Paulus,[4,5] D. Schmischke,[6] P. Swrschek,[6] and M. F. Kling[1,3]

[1]*Max-Planck-Institut für Quantenoptik, Hans-Kopfermann-Straße 1, D-85748 Garching, Germany*
[2]*Physical Chemistry, Freie Universität Berlin, Takustr. 3, D-14195 Berlin, Germany*
[3]*J. R. Macdonald Laboratory, Department of Physics, Kansas State University, Manhattan, Kansas 66506, USA*
[4]*Friedrich-Schiller-Universität Jena, Max-Wien-Platz 1, D-07743 Jena, Germany*
[5]*Helmholtz Institut Jena, D-07743 Jena, Germany*
[6]*GS Vitec GmbH, Mittelgründauer Str.21a, D-63584 Gründau, Germany*

(Received 29 June 2011; accepted 25 August 2011; published online 28 September 2011)

High-speed, single-shot velocity-map imaging (VMI) is combined with carrier-envelope phase (CEP) tagging by a single-shot stereographic above-threshold ionization (ATI) phase-meter. The experimental setup provides a versatile tool for angle-resolved studies of the attosecond control of electrons in atoms, molecules, and nanostructures. Single-shot VMI at kHz repetition rate is realized with a highly sensitive megapixel complementary metal-oxide semiconductor camera omitting the need for additional image intensifiers. The developed camera software allows for efficient background suppression and the storage of up to 1024 events for each image in real time. The approach is demonstrated by measuring the CEP-dependence of the electron emission from ATI of Xe in strong ($\approx 10^{13}$ W/cm^2) near single-cycle (4 fs) laser fields. Efficient background signal suppression with the system is illustrated for the electron emission from SiO_2 nanospheres. © *2011 American Institute of Physics*. [doi:10.1063/1.3639333]

I. INTRODUCTION

Few-cycle optical laser fields with well-defined electric field waveforms permit the control of electron dynamics on attosecond time scales. Detailed knowledge of the control of electron dynamics in multi-electron systems and its real-time observation are of great scientific interest and drive current research efforts in attosecond physics.[1] Imaging techniques such as velocity-map imaging (VMI)[2] or reaction microscopy (REMI),[3] which provide the momentum distributions of charged particles, have been successfully employed in recent studies on the control (and partly also real-time observation) of electrons in atoms,[4–7] molecules,[8–15] and nanostructures.[16] In the majority of these studies, the electric field waveform $E(t) = E_0(t)\cos(\omega t + \phi)$ of the employed laser pulses with amplitude $E_0(t)$, frequency ω, and carrier-envelope phase (CEP) ϕ was actively stabilized via CEP locking. Despite significant progress in phase stabilization technology,[17] the maximum duration of continuous phase stabilization of amplified laser systems is typically a few hours.

This limitation has triggered efforts to measure the CEP for every single laser shot rather than stabilizing it. Recently, Wittmann *et al.* reported on the first measurement of the CEP for every single laser shot of an amplified 3 kHz few-cycle laser system employing the stereographic detection of electrons from the above-threshold ionization (Stereo-ATI) of rare gases.[18] This pioneering study has been significantly furthered in recent work on the real-time determination of the CEP[19,20] and determination of the pulse duration of the laser pulses.[21] Only very recently, the first implementation of this technology for the tagging of the CEP in another, simultaneously conducted experiment was reported.[5] In this study, a REMI was combined with CEP-tagging to measure the CEP-dependence of the non-sequential double ionization of Ar.

While both REMI and VMI are capable of measuring the momentum distributions of charged fragments, they have individual advantages and disadvantages, justifying their choice for an experiment:

1. REMI allows the detection of particles in coincidence. Typically, a cold gas target is required in order to achieve sufficient momentum resolution. The number of hits that can be recorded by the detectors per laser shot is limited (up to a few hits on the ion and the electron detector). These restrictions result in count rates of a few per laser shot (or less than one if coincidence detection is used).
2. In VMI, the density of the gas target is mostly limited by the occurrence of space charge effects and may be limited by the need to maintain sufficiently low pressures to operate a microchannel plate (MCP) detector. The number of hits onto the detector per laser shot can be many orders of magnitude higher than for a REMI (and may eventually be limited by the damage threshold of the detector).

Generally, if coincident detection of multiple charged particles is required, the use of a REMI is desirable. If coincident detection is not needed, VMI is a good choice as it allows for much higher count rates and, thus, shorter acquisition times and better statistics. Consequently, a large number of studies on the imaging of the attosecond control of electron dynamics have been conducted employing VMI.

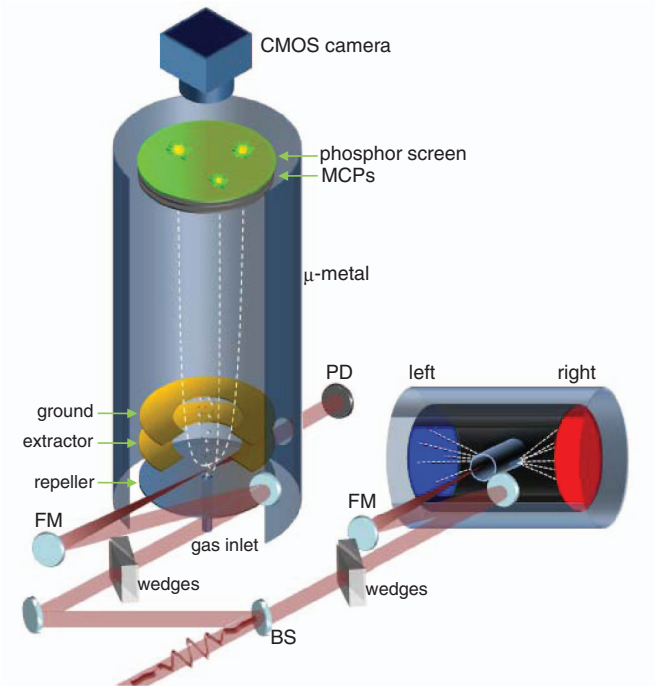

FIG. 1. (Color online) Experimental setup including both VMI (left) and Stereo-ATI (right). A broadband beam splitter (BS) provides two laser beams. One beam is focused by a 50 cm focal length spherical mirror (FM) into the VMI chamber, where the photoemitted electrons are projected by an electrostatic lens onto the MCP/phosphor screen detector and recorded by a CMOS camera. The second beam is focused by a 25 cm focal length spherical mirror into the Stereo-ATI. Electrons generated in the focus are detected by MCP stacks located to the left and right of the laser polarization axis (horizontal). A common trigger for the setup is derived from a fast photodiode (PD). The pulse duration for the VMI and Stereo-ATI parts of the setup can be optimized individually by the insertion of dispersive material using pairs of fused silica wedges.

Here, we report on the first implementation of single-shot phase tagging combined with single-shot high-speed (1 kHz repetition rate) velocity-map imaging recording up to 1024 events per laser shot. We employ a complementary metal-oxide semiconductor (CMOS) camera of the newest generation providing higher sensitivity than used in previous studies[22] and, therefore, omitting the need for an additional image intensifier. The setup can be utilized in studies of attosecond light-wave control of electron dynamics as well as numerous other CEP-dependent effects, without the need for CEP stabilization. The approach is demonstrated by measuring the CEP-dependence of the above-threshold ionization of Xe and the electron emission from SiO_2 nanoparticles in strong, nearly single-cycle (4 fs) laser fields.

II. EXPERIMENTAL SETUP

The setup for the single-shot velocity-map imaging alongside Stereo-ATI phase-tagging is schematically shown in Fig. 1. Laser pulses with a central wavelength of 720 nm were split into two parts by a broadband 20/80 beam splitter (BS). Both beams passed through pairs of wedges for individual minimization of pulse duration for both the VMI and the Stereo-ATI experiment to about 4 fs. The more intense beam was focused with a 50 cm focal length spherical mirror into an effusive atomic jet in the center of the ion optics of the VMI spectrometer. The intensity of the laser field was adjusted by a continuously variable neutral density filter. The gas for the VMI of ATI in Xe was introduced into the ultrahigh vacuum experimental chamber through a 100 μm diameter hole in the center of the repeller plate (see Fig. 1) forming an effusive gas jet. The typical operating pressure in the experimental vacuum chamber with the gas load was 2×10^{-6} mbar for a background pressure of 2×10^{-7} mbar. Electrons emitted by the ionization of the Xe target were projected by a static electric field onto a MCP/phosphor screen detector (Hamamatsu F2226-24PX) and the resulting images were recorded by a high-speed, 1280 $\times$ 1024 pixel CMOS camera (GSVitec). The polarization of the laser field was parallel to the detector plane. To reduce background contributions, the voltage across the MCP was gated using a high-voltage switch with a gate width of 60 ns.

The image acquisition of the CMOS camera was synchronized to the laser. The trigger for the camera (as well as for the Stereo ATI and computer data acquisition) was given by a transistor-transistor logic pulse generated by a constant fraction discriminator fed by a fast photodiode. The exposure time for each single image was set to 100 ms. The bottleneck in taking images at such high repetition rates is the storage of the image data, especially if longer acquisition times are desired. This makes real-time data processing unavoidable. With the current setup, up to 1024 pixels per laser shot can be stored on the computer at 1 kHz repetition rate (corresponding to 1024 events if an electron hit results in the illumination of a single pixel). Figure 2 outlines the data acquisition process. The CMOS camera acquires images at the laser repetition rate. The signal bandwidth between camera and computer requires a reduction of the image size to 800 $\times$ 600 pixels. The data is transferred to the computer where it is post-processed by the camera control software (GSVitec MARATHON PRO). We have developed and implemented a new routine into the software that allows to save only those pixel information (position and intensity) above a defined threshold level to the hard disk. The threshold value can be chosen arbitrarily. Since the camera does not exhibit a uniform background level and intensity response across the CMOS chip, flat-field correction is applied for each individual frame with a previously acquired bias image. As can be seen in Fig. 2, the flat-field correction improves the signal-to-noise ratio considerably. This method results not only in a drastic reduction of the amount of data that needs to be stored but also in a nearly noise-free measurement. As electron hits on the MCP are sufficiently more intense than the background noise from the CMOS and MCP (see Fig. 2(c)), nearly all unwanted counts in the measurements can be suppressed. Additionally, the gating of the MCP minimizes the number of dark counts during the exposure time. Using the outlined background suppression scheme, the need for protection of the CMOS camera system from ambient light sources can be omitted.

It should be noted that the image quality was found to be very sensitive to the alignment of the camera and proper adjustment of the focusing lens of the camera. An inhomogeneous focus across the image creates asymmetric images due to the thresholding algorithm. With proper alignment, such

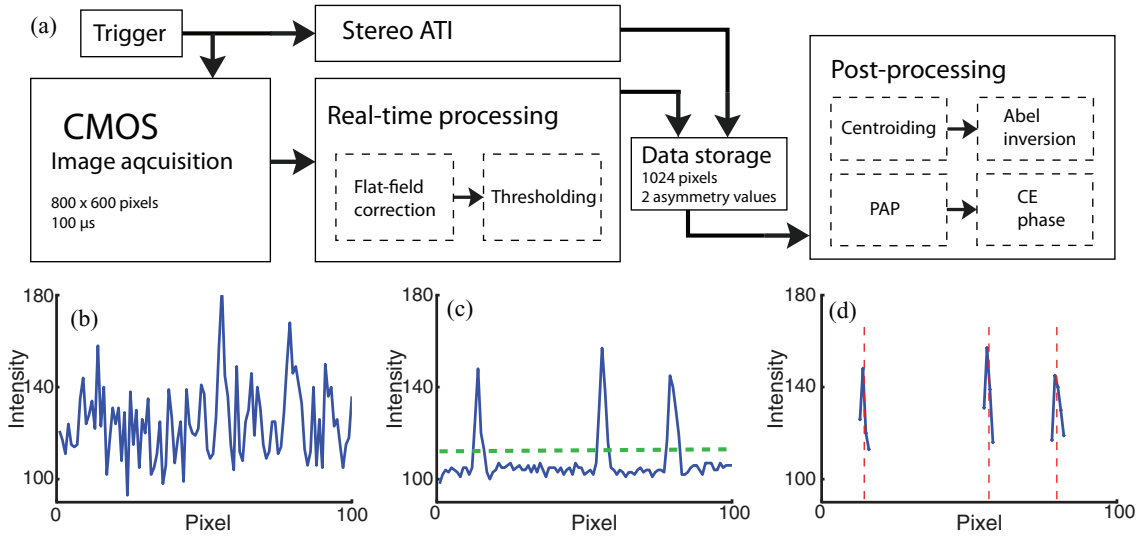

FIG. 2. (Color online) (a) Diagram of the image data processing. (b) CMOS line scan for a raw single-shot image. (c) Flat-field corrected line scan. The dashed line represents the threshold value. (d) Pixel information (above threshold) transferred to the computer. The centers of gravity are indicated by the dashed lines.

single-shot artifacts can be avoided. To align the camera to the laser beam, the electrostatic lenses were set to the spatial imaging mode of the spectrometer and the CMOS camera was adjusted until the line formed by photoelectrons generated within the laser focal region was parallel to the CMOS camera.

In order to facilitate single-shot carrier-envelope phase-tagging alongside VMI, the second part of the laser beam (see Fig. 1) was sent into a Stereo-ATI phase meter.[18] The phase meter and single-shot phase tagging were described earlier.[5,18,20] Briefly, two time-of-flight (TOF) spectra for ATI electrons emitted from Xe are recorded along both directions of the laser polarization axis (left and right detector in Fig. 1). The CEP is determined via a measurement of the recollision electrons from the ATI process, which are sensitive to the CEP of a short laser pulse. By means of two properly adjusted gated integration regions of the TOF spectra (see Wittmann *et al.*[18] for details), two asymmetry values, $A_{1,2} = (L_{1,2} - R_{1,2})/(L_{1,2} + R_{1,2})$, are determined by an electronic circuit,[20] where L and R are related to the number of electrons detected by the left and right detectors, respectively. Analog voltage signals corresponding to the asymmetry values are recorded by the computer. A parametric asymmetry plot (PAP) of A_1 vs A_2 can be generated, in which the polar angle, θ, corresponds to the measured CEP, ϕ_{exp}, exhibiting an offset, ϕ_0, with respect to the absolute CEP, ϕ: $\theta \approx \phi_{exp} + \phi_0$ (see, e.g.,[5,18,20] for details). A master trigger synchronizes the data acquisition of the asymmetry values to the acquisition of the single-shot velocity-map images. The asymmetry values not only contain information about the CEP but also the intensity[20] and pulse duration,[21] which can be used in the analysis of the VMI images.

III. SINGLE-SHOT VMI

Figure 3(a) shows a typical raw image obtained from ATI of Xe atoms with a single laser pulse. The laser intensity was 2.5×10^{13} W/cm^2 and the polarization axis of the laser field was set along the p_y axis. The image consists of individual spots (groups of pixels), where each spot corresponds

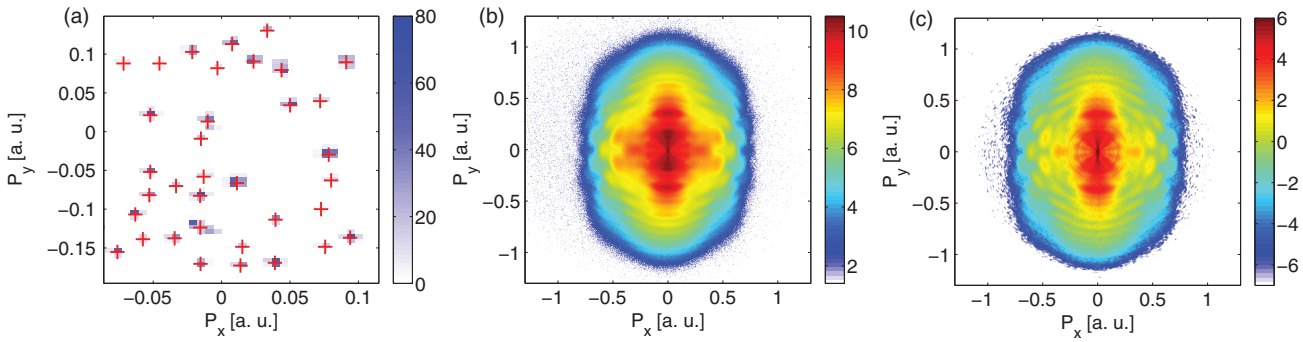

FIG. 3. (Color online) (a) Single-shot image (projected along p_z) of electron emission from ATI in Xe. The intensity is plotted on a linear scale. The laser polarization was set along the p_y axis. The crosses denote the centers of gravity of each electron hit. (b) Logarithmic plot of the sum of electron events over $\sim 10^6$ single-shot images (projected along p_z). (c) A cut through the photoelectron momentum distribution at $p_z = 0$, obtained from (b) by applying an iterative inversion procedure.

to a single electron hitting the MCP detector. Since, in principle, single-shot imaging allows for determining the number of electrons that were recorded in total (under the condition that no hits overlap directly), it is worthwhile to consider a more quantitative analysis. Depending on the magnification setting of the imaging lens, a single electron hit on the MCP can extend over several pixels of the CMOS chip (see Fig. 3(a)). To further increase the resolution of the VMI measurement, a centroiding algorithm can be applied during post-processing of the image data. Using the (background corrected) intensity information, the algorithm calculates the center of gravity of each individual hit and, thus, provides sub-pixel resolution. The sum over 10^6 of such single, post-processed images (taking slightly less than 17 min at 1 kHz repetition rate) is presented in Fig. 3(b). To reconstruct a cut through the 3D momentum distributions of the electron emission from the 2D projections recorded by the camera, an iterative inversion method was used.[23] Fig. 3(c) shows a cut (at $p_z = 0$) through the 3D photoelectron momentum distribution. The electron angular distribution is similar to what was observed in earlier experiments.[4] The central part of the image consists of the directly emitted electrons, while the higher electron energy part results from electrons that are driven back by the laser field to the ion and (re)scatter. The classical cutoff of backscattered electrons is $10U_p$, where U_p is the ponderomotive potential of an electron in the laser field. The centroiding approach is useful for certain settings of the magnification by the lens system and electron count rate (determined by the laser intensity and target density). If the magnification is set very low, single electrons light up essentially a single pixel such that centroiding may not be needed. Furthermore, if the ionization rate is chosen high, overlapping events would be counted by the centroiding algorithm as a single event, which results in a distortion and wrong count rates, especially in the center of the images. With a laser intensity of 2.5×10^{13} W/cm^2, only 150 electrons are detected on average and the corresponding bright pixel groups for each electron hit are typically spatially well separated on the detector.

IV. PHASE TAGGING

It is well known that the direction of ATI electrons generated by few-cycle fields can be efficiently controlled by the CEP.[24] Figure 4 (center) shows a PAP of ~5000 non-phase-stabilized laser shots recorded by the Stereo-ATI phase meter. The CEP can be derived from the polar angle with respect to the origin. One has to note that a rebinning of the data is necessary (according to the procedure described in Ref. 20) and yields more reliable CEP information. Using the measured PAP data to tag the single-shot VMI allows the creation of summed VMI images for a certain CEP range. The minimal size of the CEP bins is only determined by the accuracy of the Stereo-ATI setup and acquisition time in terms of statistical significance. Figure 4 (outside) shows the sum of images recorded within four selected phase intervals (as indicated in the PAP). The difference of the momentum distribution of the electron emission process can be seen.

To further quantify the CEP-dependence of the electron emission process, an asymmetry parameter, a, can be

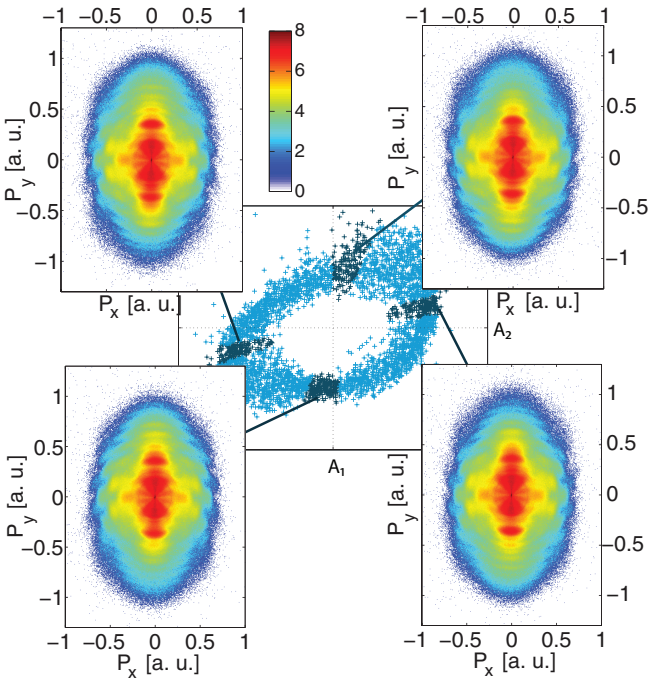

FIG. 4. (Color online) Center: Parametric asymmetry plot obtained with the single-shot Stereo-ATI for 5000 non-phase-stabilized laser shots. Outside: Summed VMI images (projected along p_z) for four different CE phases over 5×10^4 shots each; the corresponding CE phases are highlighted in the PAP.

defined by the number of electron hits, such that $a = (n_+ - n_-)/(n_+ + n_-)$. Here, n_+ is the number of electron hits with momentum $p_y > 0$ and n_- is the corresponding number for momentum $p_y < 0$. Figure 5(a) shows the asymmetry as a function of momentum along the laser polarization axis, p_y, and CEP. Here, the asymmetry value was obtained by integrating over events within an angle of $\pm 15^\circ$ to the p_y axis. To fully explore the sensitivity of our setup, we also examined smaller regions in the VMI images. The phase dependence for a certain position in momentum space can be expressed as $a(\phi) = a_0 \cos(\phi_{exp} + \Delta\phi)$, where a_0 is the asymmetry amplitude and $\Delta\phi$ is the phase shift of the asymmetry oscillation with CEP. Note, however, that ϕ_{exp} is the phase measured by the Stereo-ATI and can be offset to the absolute CEP in the VMI by the constant term ϕ_0. The expression for a was fitted to the experimental data for a bin size of 2×2 pixels. Figures 5(b) and 5(c) show maps of a_0 and $\Delta\phi$ for the inverted VMI data. As expected, electrons in the cutoff region show the highest asymmetry amplitude. Slower electrons exhibit complex structure both in amplitude and phase shift.

V. ELECTRON EMISSION FROM SiO_2 NANOSPHERES

To illustrate one of the advantages of the developed phase-tagged, single-shot VMI, we measured the electron emission from 90 nm SiO_2 nanospheres. The setup for the injection of the nanoparticles is identical to the one employed in Ref. 16. The nanoparticle target is delivered to the interaction region by an aerodynamic lens.[16,25–27] This method employs the vaporization of a low concentration solution of nanoparticles contained in a solvent (here ethanol) by a carrier gas

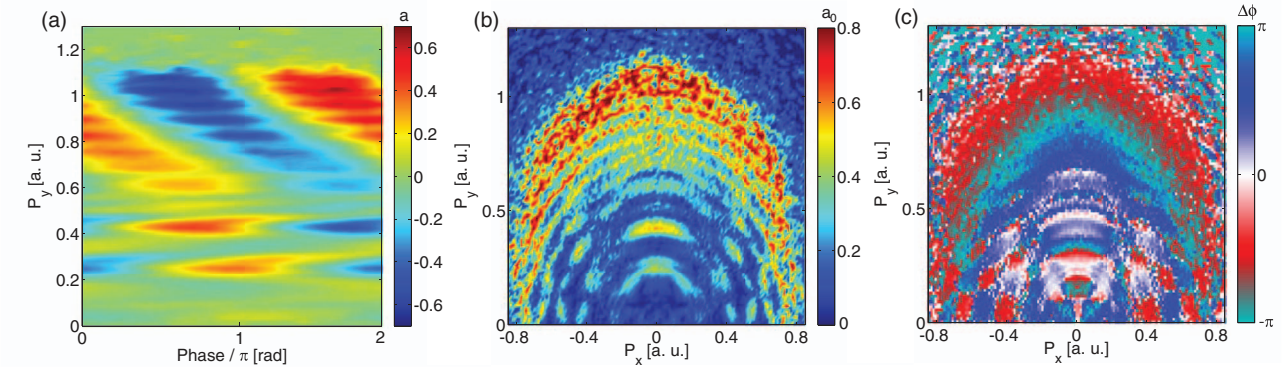

FIG. 5. (Color online) (a) Asymmetry map as a function of momentum along the polarization axis and CEP. (b) Asymmetry amplitude a_0 and (c) phase shift, $\Delta\phi$, of its oscillation with CEP as a function of electron momentum in the x- and y-direction.

(here N_2). The vapor is dried before insertion into the aerodynamic lens. Residual carrier gas is removed by differential pumping after the last aperture of the aerodynamic lens. Typical particle densities that can be reached in the focus with such a source are in the range of 10^6 particles/cm^3.[25] In the experiment, typically 0–1 nanoparticles are hit within a single laser shot. Consequently, a considerable number of laser shots contains only background ATI signal from the residual carrier gas.

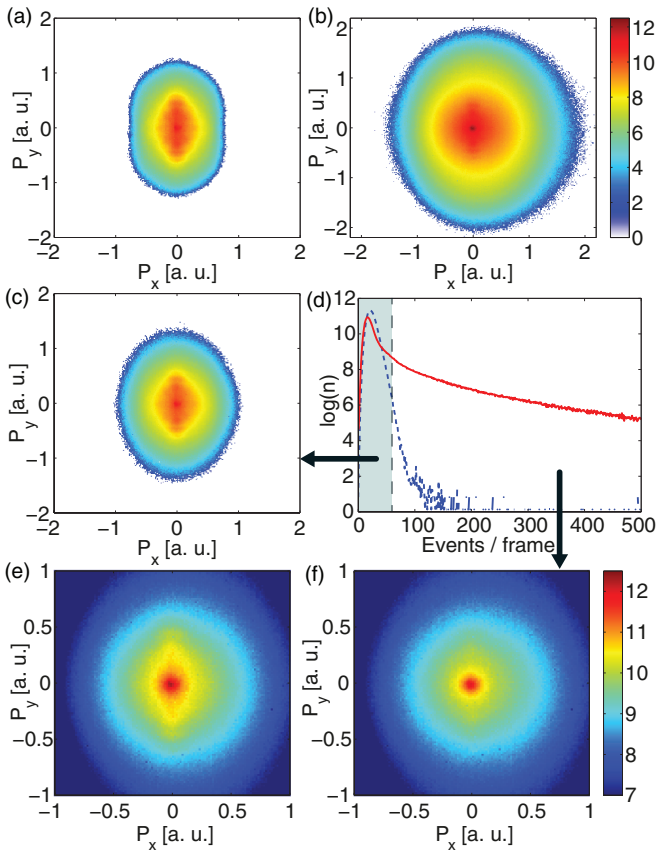

FIG. 6. (Color online) Integrated VMI image (projected along p_z) acquired with (a) pure ethanol and (b) 90 nm diameter SiO_2 nanospheres in ethanol. The color scale is logarithmic. (c) Measurement with nanoparticles considering laser shots with event numbers of 62 and below per image. (d) Histograms of the event numbers per image for the measurement with (solid line) and without (dashed line) nanoparticles. Measurement with nanoparticles considering all laser shots (e) and just the laser shots with event numbers larger than 62 (f).

In contrast to Ref. 16, where multi-shot VMI measurements were performed with phase-stabilized pulses, the approach introduced here allows to analyze the images recorded for each individual laser shot and remove the unwanted background during post-processing. Figures 6(a) and 6(b) show VMI images (projected along p_z) that were acquired for 1.71×10^6 laser shots at a peak intensity of 3.1×10^{13} W/cm^2 with pure ethanol and a dispersion of 90 nm diameter SiO_2 nanospheres in ethanol (at a concentration of 2 g/l), respectively. Figure 6(a), therefore, contains only the background signal while Fig. 6(b) contains both the desired signal from the nanoparticles as well as the background. It can be seen that the high-momentum part of the SiO_2 spectra is free from any background contributions; however, at momenta below 1.2 a.u., both signals overlap.

Figure 6(d) shows a histogram of the event count for the measurement with the nanospheres (solid line), which is compared to the measurement with just background (dashed line). Since the background produces a relatively low number of electrons per laser shot, the histogram was divided into images with a low number of events per frame (shaded area with an upper limit at 62 events/frame, including 99.8% of all events in the ethanol data) and data with higher numbers. The images for the shaded, low-count region were summed up and the result, shown in Fig. 6(c), largely resembles the background (see Fig. 6(a)). In Figs. 6(e) and 6(f), we zoomed into the low momentum part of the measurement with the nanoparticles considering all laser shots and just the laser shots with event numbers larger than 62, respectively. A strong suppression of the background ATI structure can be seen in Fig. 6(f), where the laser shots containing predominantly background have been excluded. The single-shot technique introduced here, therefore, permits an efficient and straightforward background suppression scheme for thin nanoparticle targets, which is a challenge otherwise.

VI. CONCLUSIONS AND OUTLOOK

In this paper, single-shot VMI detection combined with CEP-tagging at a repetition rate of 1 kHz is demonstrated. Using a high-speed, sensitive CMOS camera, single-shot VMI

images were recorded, and real-time image processing allowed the storage of up to 1024 events per image. Using our specially developed software for this task, a standard desktop computer was capable of handling the acquisition and storage of the experimental data, even for extended scans. With this setup, VMI measurements of the CEP-control of electron dynamics employing ultrashort pulses is greatly simplified as there is no need for CEP-stabilization. The direct measurement of the CEP also guarantees a higher precision as compared to phase stabilization (see, e.g., Refs. 5 and 20). In addition, much more information can be retrieved from the single-shot experimental data during analysis. For nanoparticle experiments, the contribution from the carrier gas could successfully be suppressed. Single-shot measurements also permit subsequent sorting of the data based on additional experimental parameters, e.g., intensity and pulse duration, which may vary on a shot-to-shot basis, thereby enabling VMI measurements with unprecedented accuracy. The technique is not limited to the analysis of photoelectrons but can also be applied to ions which could be useful for studying, e.g., the localization and control of electrons in molecules by means of ultrashort laser pulses.

ACKNOWLEDGMENTS

We are grateful to Ferenc Krausz and Marc Vrakking for their support and for making specialized equipment available to us. We acknowledge experimental support by Tim Rathje, Sergei Trushin, Izhar Ahmad, and Christoph Skrobol. Financial support from the Chemical Sciences, Geosciences, and Biosciences Division, Office of Basic Energy Sciences, Office of Science, U.S. Department of Energy, the National Science Foundation under CHE-0822646, the LaserLab Europe, the DFG via the Emmy-Noether program SPP1391 (Grant No. PA 730/4), the International Collaboration in Chemistry program, and the Cluster of Excellence: Munich Center for Advanced Photonics (MAP) is gratefully acknowledged.

[1]F. Krausz and M. Ivanov, Rev. Mod. Phys. **81**, 163 (2009).
[2]A. Eppink and D. Parker, Rev. Sci. Instrum. **68**, 3477 (1997).
[3]J. Ullrich, R. Moshammer, A. Dorn, R. Dörner, L. P.H. Schmidt, and H. Schmidt-Böcking, Rep. Prog. Phys. **66**, 1463 (2003).
[4]M. F. Kling, J. Rauschenberger, A.-J. Verhoef, E. Hasović, T. Uphues, D. B. Milošević, H. G. Muller, and M. J. J. Vrakking, New J. Phys. **10**, 025024 (2008).
[5]N. G. Johnson, O. Herrwerth, A. Wirth, S. De, I. Ben-Itzhak, M. Lezius, B. Bergues, M. F. Kling, A. Senftleben, C. D. Schröter, R. Moshammer, J. Ullrich, K. J. Betsch, R. R. Jones, A. M. Sayler, T. Rathje, K. Rühle, W. Müller, and G. G. Paulus, Phys. Rev. A **83**, 013412 (2011).
[6]X. Liu, H. Rottke, E. Eremina, W. Sandner, E. Goulielmakis, K. O. Keeffe, M. Lezius, F. Krausz, F. Lindner, M. Schätzel, G. G. Paulus, and H. Walther, Phys. Rev. Lett. **93**, 263001 (2004).
[7]J. Mauritsson, T. Remetter, M. Swoboda, K. Klünder, A. L'Huillier, K. J. Schafer, O. Ghafur, F. Kelkensberg, W. Siu, P. Johnsson, M. J. J. Vrakking, I. Znakovskaya, T. Uphues, S. Zherebtsov, M. F. Kling, F. Lépine, E. Benedetti, F. Ferrari, G. Sansone, and M. Nisoli, Phys. Rev. Lett. **105**, 053001 (2010).
[8]M. F. Kling, C. Siedschlag, A. J. Verhoef, J. I. Khan, M. Schultze, T. Uphues, Y. Ni, M. Uiberacker, M. Drescher, F. Krausz, and M. J. J. Vrakking, Science **312**, 246 (2006).
[9]M. F. Kling, C. Siedschlag, I. Znakovskaya, A. Verhoef, S. Zherebtsov, F. Krausz, M. Lezius, and M. J. J. Vrakking, Mol. Phys. **106**, 455 (2008).
[10]M. Kremer, B. Fischer, B. Feuerstein, V. L.B. de Jesus, V. Sharma, C. Hofrichter, A. Rudenko, U. Thumm, C. D. Schröter, R. Moshammer, and J. Ullrich, Phys. Rev. Lett. **103**, 213003 (2009).
[11]I. Znakovskaya, P. von den Hoff, S. Zherebtsov, A. Wirth, O. Herrwerth, M. J. J. Vrakking, R. de Vivie-Riedle, and M. F. Kling, Phys. Rev. Lett. **103**, 103002 (2009).
[12]Y. Liu, X. Liu, Y. Deng, C. Wu, H. Jiang, and Q. Gong, Phys. Rev. Lett. **106**, 073004 (2011).
[13]B. Fischer, M. Kremer, T. Pfeifer, B. Feuerstein, V. Sharma, U. Thumm, C. D. Schröter, R. Moshammer, and J. Ullrich, Phys. Rev. Lett. **105**, 223001 (2010).
[14]I. Znakovskaya, P. von den Hoff, N. Schirmel, G. Urbasch, S. Zherebtsov, B. Bergues, R. de Vivie-Riedle, K.-M. Weitzel, and M. F. Kling, Phys. Chem. Chem. Phys. **13**, 8653 (2011).
[15]G. Sansone, F. Kelkensberg, J. F. Pérez-Torres, F. Morales, M. F. Kling, W. Siu, O. Ghafur, P. Johnsson, M. Swoboda, E. Benedetti, F. Ferrari, F. Lépine, J. L. Sanz-Vicario, S. Zherebtsov, I. Znakovskaya, A. L'Huillier, M. Y. Ivanov, M. Nisoli, F. Martín, and M. J. J. Vrakking, Nature (London) **465**, 763 (2010).
[16]S. Zherebtsov, T. Fennel, J. Plenge, E. Antonsson, I. Znakovskaya, A. Wirth, O. Herrwerth, F. Süßmann, C. Peltz, I. Ahmad, S. A. Trushin, V. Pervak, S. Karsch, M. J. J. Vrakking, B. Langer, C. Graf, M. I. Stockman, F. Krausz, E. Rühl, and M. F. Kling, Nat. Phys. **7**, 656 (2011).
[17]S. Koke, C. Grebing, H. Frei, A. Anderson, A. Assion, and G. Steinmeyer, Nature Photon. **4**, 462 (2010).
[18]T. Wittmann, B. Horvath, W. Helml, M. G. Schätzel, X. Gu, A. L. Cavalieri, G. G. Paulus, and R. Kienberger, Nat. Phys. **5**, 357 (2009).
[19]Z. Chen, T. Wittmann, B. Horvath, and C. Lin, Phys. Rev. A **80**, 061402(R) (2009).
[20]A. M. Sayler, T. Rathje, W. Müller, K. Rühle, R. Kienberger, and G. G. Paulus, Opt. Lett. **36**, 1 (2011).
[21]A. M. Sayler, T. Rathje, W. Müller, C. Kürbis, K. Rühle, G. Stibenz, and G. G. Paulus, Opt. Express **19**, 4464 (2011).
[22]T. Horio and T. Suzuki, Rev. Sci. Instrum. **80**, 013706 (2009).
[23]M. J. J. Vrakking, Rev. Sci. Instrum. **72**, 4084 (2001).
[24]G. Paulus, F. Grasbon, H. Walther, P. Villoresi, M. Nisoli, S. Stagira, E. Priori, and S. De Silvestri, Nature (London) **414**, 182 (2001).
[25]X. Wang and P. H. McMurry, Aerosol Sci. Technol. **40**, 320 (2006).
[26]K. R. Wilson, S. Zou, J. Shu, E. Rühl, S. R. Leone, G. C. Schatz, and M. Ahmed, Nano Lett. **7**, 2014 (2007).
[27]H. Bresch, B. Wassermann, B. Langer, C. Graf, R. Flesch, U. Becker, B. Österreicher, T. Leisner, and E. Rühl, Faraday Discuss. **137**, 389 (2008).